Journal of
Ceramic Science
and Technology

J. Ceram. Sci. Tech., 02 [01] 47-54 (2011)
DOI: 10.4416/JCST2010-00019
available online at: http://www.ceramic-science.com

Influence of In-Situ Platelet Reinforcement on the Properties of Injection Moulded Alumina-Toughened Zirconia

F. Kern* **and R. Gadow**

University of Stuttgart, Institute for Manufacturing Technologies of Ceramic Components and Composites, Allmandring 7 b, D-70569 Stuttgart, Germany

received May 26, 2010; received in revised form July 05, 2010; accepted October 06, 2010

Abstract

Alumina-toughened zirconia (ATZ) materials are suitable materials for a variety of biomedical applications owing to their high strength, toughness and hydrothermal stability. The prospect of being able to offer ceramic implants to a broader group of patients requires a more cost-efficient near-net-shape manufacturing approach. Small and complex-shaped components can be efficiently mass-produced by means of ceramic injection moulding (CIM) with high surface quality and low dimensional tolerances. Compared to the state-of-the-art cold and hot isostatic pressing cycles commonly used for implant production, CIM technology does suffer from lower microstructural quality. During the thermally and rheologically transient mould-filling process, inevitably a certain number of defects are induced by flow textures, weld lines and micro-segregation. A higher level of toughness is therefore beneficial to keep strength and damage tolerance on a sufficiently high level. In order to improve thetoughness of ATZ, *in-situ* platelet reinforcement with strontium hexaaluminate precipitates was introduced. The influence on processing behaviour, strength and toughness of as-manufactured and final-machined platelet-containing and platelet-free 2.5Y-TZP/15 vol% alumina composites was investigated. Platelets improve the mechanical properties. Weibull statistics show that platelet addition leads to drastic improvements in reliability.

Keywords: ATZ, CIM, platelets, Weibull statistics, toughening

I. Introduction

Yttria-stabilized zirconia ceramics are materials commonly used for biomedical implants owing to their high level of strength, toughness and bioinertness [1]. Application in hip implants has, however, suffered some drawbacks caused by hydrothermal aging. Even if processed correctly, Y-TZP does markedly transform from tetragonal to monoclinic phase as soon as it is exposed to body fluids for a longer period of time. This phase transformation is associated with a volume expansion that starts at the surface and progresses into the bulk [2]. Recent results show that the process is not only caused by hydrolysis of yttrium oxide and a loss in stabilization but also by the creation of residual stresses by transformed grains [3, 4]. Tsubakino has shown that alumina addition to Y-TZP improves the hydrothermal stability [5]. Ross *et al.* showed that small amounts of alumina < 0.15 % built in at the grain boundary of Y-TZP do change the concentration profiles of yttria considerably [6]. Alumina is therefore added in a low percentage by Y-TZP powder manufacturers to assure higher long-term stability *in vivo*. Alumina addition in larger fractions > 10 % leads to alumina-toughened zirconia (ATZ). Tsukuma has shown that ATZ can reach higher levels of strength than Y-TZP [7]. Bending strength levels of 2.4 GPa were reported in hot-isostatic-pressed material. *In-situ* platelet toughening was introduced by Cutler to improve the strength and retain the toughness of Ce-TZP-based ATZ [8]. Platelets were grown by *in-situ*-reacting of strontium zirconate with alumina to yield strontium hexaaluminate $SrAl_{12}O_{19}$. The strontium aluminate forms hexagonal platelets of 5 – 10 µm in size that can deflect and bridge cracks and thus lead to higher toughness. Cutler reported failure to produce platelet-reinforced Y-TZP composites. Some mechanistic evidence on formation of lanthanum hexaaluminate platelets was presented by Miura [9]. Burger successfully applied the concept to zirconia- toughened alumina [10].

Ceramic injection moulding is an established technology for manufacturing small- and medium-size ceramic components with complex geometry, which cannot be economically produced by axial pressing. Complementary to these potential economic advantages are process-immanent problems such as higher flaw populations. These microstructural defects can be minimized with sophisticated processing techniques such as high-energy mixing of the feedstocks and proper mould design but not completely avoided. It was shown that e.g. ZTA ceramics produced by CIM with subsequent pressureless sintering showed typical defect sizes in the range between 10 – 15 µm [11]. According to Griffith's law, a flaw size of 10 µm requires a fracture toughness of 6.3 MPa·√m in order to achieve a strength level of 1000 MPa. Additional toughness thus directly increases the strength in TZP materials with transforma-

* Corresponding author: frank.kern@ifkb.uni-stuttgart.de

tion limited strength. Swain has shown that this assumption is valid up to $K_{IC} \sim 8$ MPa·√m. Then the fracture behaviour shifts to R-curve dominated behaviour [12]. Casellas has shown that fully tetragonal 2.5Y-TZP has moderate toughness of ~ 4 - 4.25 MPa·√m and an almost negligible R-curve behaviour [13]. Reducing the defect sizes by post-HIPing is a proven strategy to improve the mechanical properties; this additional heat treatment does, however, increase the cost. For biomedical implants, HIP treatment is considered mandatory not only for achieving improved mechanical properties, but mainly to avoid the penetration of body fluid into flaws and other surface defects that can be present in pressurelessly sintered ceramics.

In this study the feasibility of producing platelet-reinforced and conventional ATZ with 15 vol% alumina was investigated for the first time with the aim of applying the technology for improving the performance and reliability of injection-moulded components for biomedical applications.

II. Experimental

Injection moulding feedstocks were produced from commercially available powders. The raw materials and their properties are listed in Table 1. In order to improve toughness without losing stability against spontaneous transformation, an yttria content of 2.5 mol% in the TZP was adjusted by mixing TZ-3Y-SE and TZ-0 powders. Alumina content was set at 15 vol% (ATZ15), the second feedstock (ATZ15P) contained strontium zirconate powder sufficient to convert 5 vol% of alumina to strontium aluminate platelets during sintering. The platelet content was limited because it was expected that higher platelet fractions would negatively affect densification behaviour in pressureless sinteringowing to the high aspect ratio of the platelets. 15 mass% (48 vol%) of thermoplastic binder (Licomont EK 583 G, Embemould, Germany) were used for preparation of the feedstock. The procedure of feedstock preparation is described elsewhere in detail [11]. Powder and binder were mixed at 140 °C in a two stage compounding process with a premixing step in a double-sigma blade kneader (Linden, Marienheide, Germany) and a subsequent high-torque mixing step in a twin-screw extruder (Thermofisher Scientific, Karlsruhe, Germany). Testing samples were produced in a mould with exchangeable cavities. Bending bars (3 x 4 x 35 mm^3) were injected through a pin-point gate against a withdrawing plunger to avoid free jet injection and flow textures, plates (3 x 30 x 40 mm) were injected through a film gate. Moulding pressure was 120 MPa for the plates and 85 MPa for the bars. Plastification temperature was set at 150 °C, mould temperature at 65 °C in both cases. Packing pressure was 40 MPa, injection speed was 20 cm^3/s. Debinding was performed as a two-stage process. The water-soluble fraction of the binder was extracted with distilled water at 60 °C overnight, samples were then dried and thermally debinded in air. Thermal debinding and presintering were performed in the same furnace. A detailed model-based approach for reliable and economically performing setting of debinding parameters for the binder used was recently presented [14]. The pore size distribution of debinded samples was studied with mercury porosimetry in order to obtain an integral value of pore sizes and a first impression on possible flaw sizes.

Table 1: Properties of selected powders.

Powder	Material	Manufacturer	Grain size [µm]*	BET surface [m^2/g]*
TZ-3YSE	tetragonal zirconia	Tosoh, Japan	0.35 (0.027)**	7±2
TZ-0	monoclinic zirconia	Tosoh, Japan	0.35 (0.027)**	14±3
APA 0.5	α-alumina	Ceralox, USA	0.3	8
$SrZrO_3$	strontium zirconate	Aldrich	< 10	n.d.

* manufacturer's specification,
** numbers in brackets: primary crystallite size

Sintering was performed based on the results of a dilatometry study. The dilatometry curves of ATZ15 and ATZ15P were measured (Netzsch STA, Selb, Germany) at three different heating rates (2,5,10 K/min). The kinetics were modelled with commercial software (Netzsch Thermokinetics, Selb, Germany). The formalism was first described by Opfermann [15]. Sintering was performed in air at 1550 °C/2 h for ATZ15 and 1525 °C/3 h for ATZ15P in an electrically heated furnace (Thermconcept , Bremen, Germany).

Sintered bars were mechanically tested as-fired without further machining. For comparison, samples prepared from plates were carefully ground with a 40-µm diamond disk and polished with 15-µm, 3-µm and 1-µm diamond suspension, edges were bevelled, cutting grooves and surface defects were removed by abrasive polishing with 15-µm diamond suspension (Struers Rotopol, Germany). For the determination of Weibull coefficients and reliable statistics, 20 bars of each type were tested. Owing to the limited sample size. 3-pt-bending tests were performed according to DIN EN 6872 with 15-mm span. Hardness was measured on five HV_{10} Vickers indents (Bareiss, Oberdischingen, Germany), Microhardness $HV_{0.1}$ and indentation modulus were measured according to the universal hardness method from loading and unloading curves on 12 indents in each case (Fischerscope, Sindelfingen Germany). Fracture toughness K_{IC} was determined with the indentation method from the indent sizes and length of wing cracks on five HV_{10} Vickers indents using the formulas of Niihara [16] and Anstis [17]. In order to verify the indentation-based results, the ISB (indentation strength in bending) method proposed by Chantikul was applied on 5 bars each with HV10 indents [18]. The phase composition of polished surfaces and of fracture surfaces was measured with XRD (Bruker D8, Germany) using Cu-Kα radiation with a monochromator, from the intensity ratios of monoclinic (111) , ($\bar{1}$11) and tetragonal (101) reflexes according to Toraya [19]. In order to quantify the initial cubic content, the intensity of reflexes in the 49.5-51.5° 2θ range were measured. Microstructures and crack paths were investigated by SEM (LEO, Cambridge, USA) on polished and thermally (1225 °C/1 h) etched surfaces. Cracks were introduced with HV_{10} indents.

III. Results and Discussion

The pore size distributions of ATZ15 and ATZ15P after debinding and presintering in air at 800 °C for 1 h are shown in Fig. 1. The main fraction of porosity is located in the range between 0.01 - 0.1 µm as can be expected from the grain sizes of the raw powders. Between 1 – 10 µm a very small (1 - 2 %) but significant amount of porosity can be detected, which is probably caused by manufacturing-related flaws. (Even if this pore-diameter-based value is not directly correlated to crack-inducing defects, the method gives a good impression of the integral value of the defect sizes to be expected.) The two materials, formed from almost identical recipes and with identical processing parameters, show no statistically relevant differences in pore size distribution. Total porosity measured was 47.9 vol% for ATZ15 and 49.8 vol% for ATZ15P, which is close to the theoretical value of 48 vol% and within expected accuracy of ± 2 %.

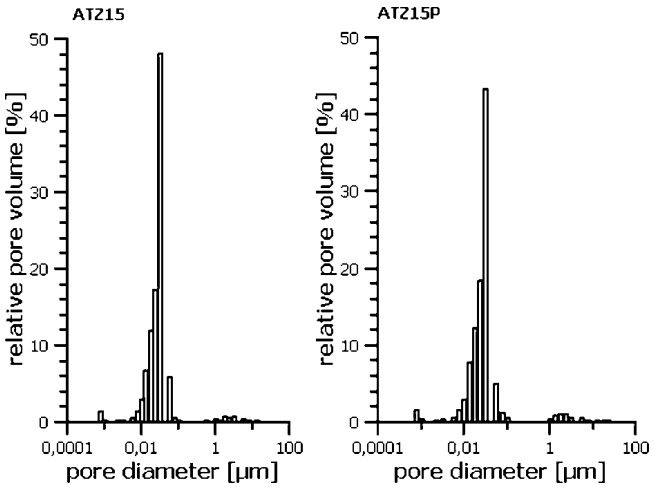

Fig. 1: Pore size distributions in ATZ15 and ATZ15P determined by mercury intrusion porosimetry.

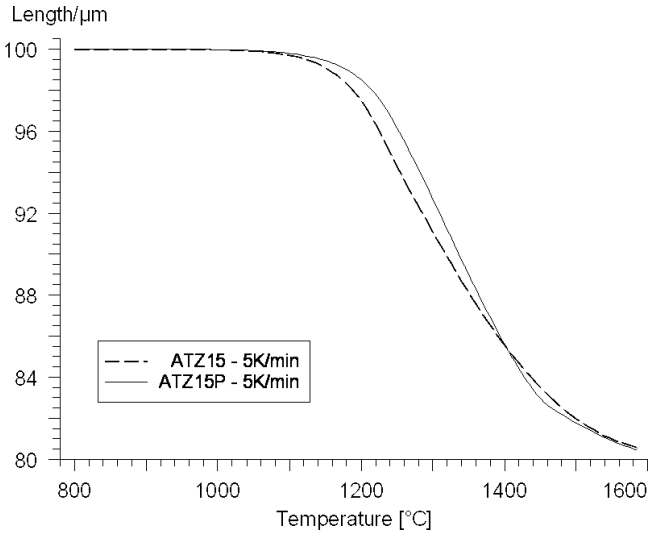

Fig. 2: Dilatometry curves of ATZ15 and ATZ15P in air at a heating rate of 5 K/min.

Modelling of the sintering kinetics reveals that both ATZ materials show similar activation energies at given densification stages. Activation energies determined by model-free estimation stay at 750-850 kJ/mol until 80 % fractional length change is reached, then the activation energies rise steeply to levels of approximately 1500 kJ/mol. This indicates that the sintering process proceeds in at least two stages, the latter being very temperature-sensitive. These results show that the addition of 15 vol% alumina lowers the sinterability of Y-TZP, which according to the manufacturer's specification is completely dense at 1450 °C/1 h. The platelet formation – at the low strontia concentration chosen – seems to have no further negative effect on densification. In fact Fig. 2 shows that at a heating rate of 5 K/min, strontium zirconate addition retards the onset of densification by ~ 20 K but slightly improves the final densification behaviour.

The sintered densities, mechanical properties and phase compositions of ATZ15 and ATZ15P are shown in Table 2. With the chosen sintering parameters both materials reach similar density. Hardness and Young's modulus are slightly higher for ATZ15. This indicates that the strontium aluminate platelets have lower hardness and Young's modulus than alumina. As expected strength of perfectly machined samples is 20 – 35 % higher for both materials than the strength of as-fired materials. Comparing ATZ15 and ATZ15P, the strength of the platelet-reinforced material is always significantly higher while the platelet-addition-related gain in toughness is moderate. The increase in average strength seems not very spectacular at first sight. The lower standard deviations of strength in case of ATZ15P hint at increased reliability. Even though the volume exposed to maximum stress is low in 3-pt.-bending compared to 4-pt-bending tests, the statistical data collected from large numbers of samples support this statement. Weibull plots are shown in Figs. 3 and 4. ATZ15, no matter if as-fired or carefully machined, reaches Weibull coefficients of n = 6.5 – 6.8. Measured values consist of a single population. In case of platelet-reinforced materials, the as-fired ATZ15P with a global Weibull coefficient of 10.7 actually shows two populations, one at high strength with a Weibull coefficient of 5.9 and one at lower strength with a Weibull coefficient of 28. The additional reinforcement by platelets cuts off the strength distribution at > 750 MPa. Platelets seem to be able to eliminate the effect of large flaws and ensure a considerable minimum strength while in ATZ15 some inferior specimens are always present. The Weibull plot of ATZ15-GP shows a very narrow distribution and an even higher Weibull coefficient of 15.9. The data points can be described by a single population even though a double-S-shape of the data points is clearly visible. It can thus be assumed that the larger flaws accounting for the lower strength of the as-fired material were eliminated by machining and that the remaining defects in the bulk are smaller and less detrimental than the surface defects in the as-fired material. Comparing the indentation toughness data shown in Table 2 with the results of the ISB test (ATZ15: $K_{IC,\,ISB}$ = 4.92 ± 0.09 [MPa·√m], ATZ15P: $K_{IC,\,ISB}$ = 5.42 ± 0.15 [MPa·√m]) shows that the indentation toughness according to Niihara is very optimistic,

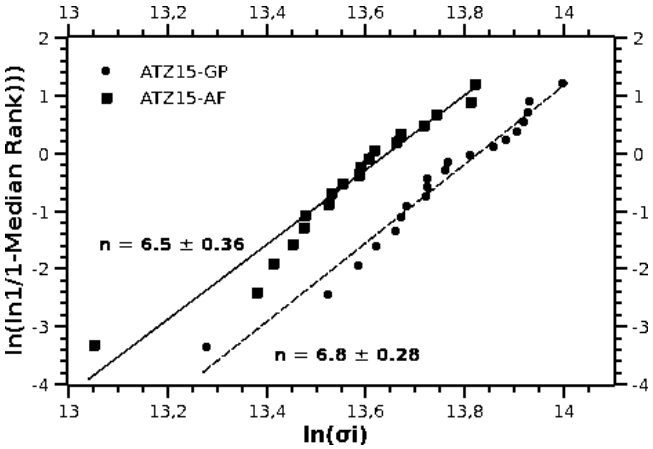

Fig. 3: Weibull plot of strength distribution in as-fired (AF) and ground and polished (GP) ATZ15.

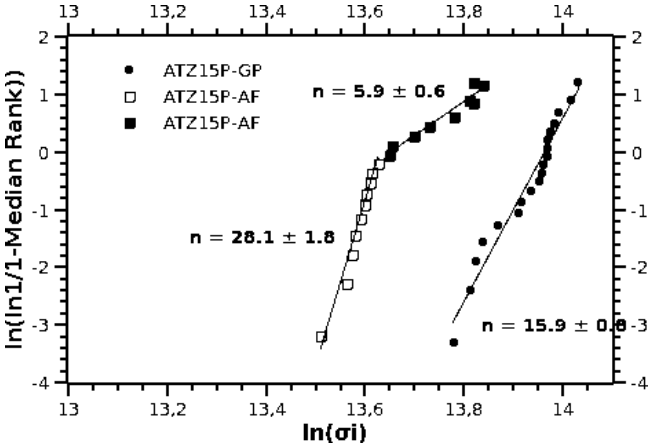

Fig. 4: Weibull plot of strength distribution in as-fired (AF) and ground and polished (GP) ATZ15P.

while the indentation toughness according to Anstis leads to identical results as the ISB-test. An estimation of critical defect size c using the Griffith criterion for brittle materials ($\sigma_F = K_{IC}/(Y\cdot\sqrt{c})$, Y = 2) and the measured values for strength σ_F and toughness K_{IC} (according to Anstis) shows that defect sizes are 10.1 µm in the as-fired and 5.8 – 6.8 µm in the machined material. Lower apparent defect sizes compared to ATZ15 are found in machined ATZ15P - apparent defect sizes as it was shown that defects in the green bodies had similar size, and sintering has led to identical density. Assuming identical defect sizes in both materials and recalculating the toughness for ATZ15P leads to the surprising result that platelet addition acts as an additional toughness increment of 0.45 MPa·√m for the ground and polished material, for the as-fired material no deviation from the measured value is observed. Evidently in order to fully exploit the potential of the platelet reinforcement it is necessary to eliminate the large surface defects by machining. Platelets can obviate the worst, but platelets will not be able e.g. to bridge cracks larger than their own size. Toughening thus depends on crack deflection and branching in as-fired materials with large surface defects.

The microstructures of ATZ15 and ATZ15P are shown in Figs. 5 and 6. As alumina content is below the percolation threshold of 16 % and intensive mixing was applied during feedstock preparation, alumina grains are isolated and well distributed. The grain size of alumina is below 1 µm, the size of zirconia grains – owing to the high sintering temperature – ranges between 0.5 – 0.7 µm in both materials. Strontium aluminate platelets in ATZ15P are randomly distributed and account for ~ 1/3 of initially added alumina as calculated. The platelets have a length of 2 – 5 µm and a thickness of < 0.5 µm. Figs. 7 and 8 show crack paths induced by Vickers indentations in ATZ15 and ATZ15P. ATZ15 shows a typical mixture of inter- and transgranular fracture with a crack path curvature defined by the size of the alumina and zirconia grains. In the platelet-reinforced material additional toughening mechanisms beside transformation toughening are active. Crack bridging, crack deflection and crack branching induced by platelets are clearly visible.

Table 2: Properties of ATZ15 sintered at 1550 °C/2 h and ATZ15 sintered at 1525 °C/3 h, (GP = ground and polished, AF = as fired).

Material	Relative density [%-th.]	Linear shrinkage [%]	Hardness HV_{10} [-]	Hardness $HV_{0.1}$ [-]	Young's modulus [GPa]
ATZ15	97.88 ± 0.54	21.7 ± 0.2	1376 ± 12	1610 ± 22	272 ± 2
ATZ15P	97.89 ± 0.2	21.7 ± 0.2	1317 ± 14	1561 ± 33	268 ± 4
	Bending strength [MPa]	Weibull-coefficient [-]	Characteristic strength [MPa]	K_{IC}, Niihara [MPa·√m]	K_{IC}, Anstis [MPa·√m]
ATZ15-GP	947 ± 150	6.8	1012	5.84 ± 0.09	4.96 ± 0.11
ATZ15-AF	781 ± 144	6.5	856		
ATZ15P-GP	1124 ± 79	15.9	1160	6.12 ± 0.17	5.41 ± 0.23
ATZ15P-AF	850 ± 83	10.7	892		

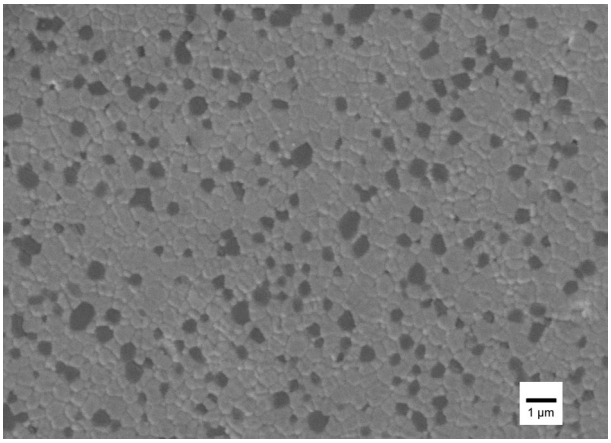

Fig. 5: SEM image of the microstructure of ATZ15, polished and thermally etched (1225 °C/1 h air) surface.

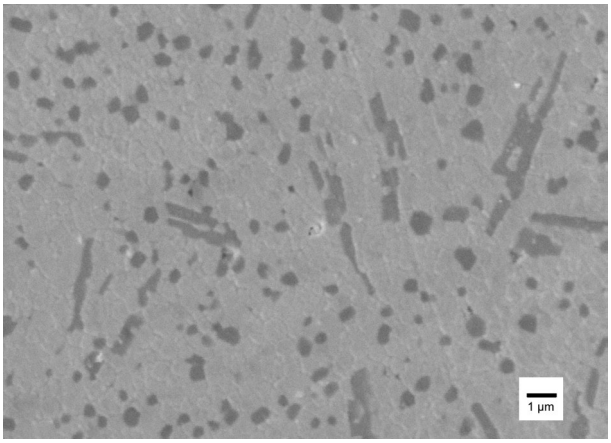

Fig. 6: SEM image of the microstructure of ATZ15P, polished and thermally etched (1225 °C/1 h air) surface.

Transformability as indicated by the moderate toughness values in both materials is not very high. It was impossible to transform the material sufficiently by rough grinding with a 250-µm diamond disk, Therefore fracture surfaces with the highest possible activation were investigated despite the poor signal-noise ratio of the rough and non-planar surfaces. As the area of the fracture faces of single broken bars was too small to obtain a good signal, the fracture surfaces of 8 - 10 bars were aligned and tested by XRD. XRD patterns of ATZ15 and ATZ15P are shown in Fig. 9. Results of phase analysis of polished and broken bars are shown in Table 3. The results of the XRD investigation clearly show that the platelets not only act as reinforcements, they also improve the transformability. ATZ15P, contrary to ATZ15,0 contains a small fraction of monoclinic phase in the as-fired condition. After fracture a higher fraction of zirconia is transformed. The transformation from tetragonal is always associated with a shift of the peaks by an increment of 0.2° to lower 2θ values owing to the generated compressive stresses. Together with monoclinic phase a considerable amount of cubic phase is formed. According to the phase diagram by Chen [20] obtained by thermodynamic modelling, cubic content at 1550 °C is low (5 – 7 %). XRD patterns of both as-sintered composites show no visible evidence of cubic phase in the 26-33° 2θ region, a few percent may be hidden in the background or as a shoulder of the tetragonal (101) reflex which coincides with the cubic (111) reflex. An investigation of the reflexes in the 49.5-51.5° 2θ region led to more concise results. The XRD pattern in the respective 2θ range is shown in Figs. 10 and 11. Cubic zirconia (JCPDS 30-1469) has a single (220) reflex at 50.18 ° while the tetragonal phase (JCPDS 79-4764) has two reflexes, (112) at 50.22° and (200) at 50.74° 2θ. The intensity ratio of the (112) and (200) reflexes is 1.865 for purely tetragonal material. In presence of cubic phase the $(112)_t$+$(220)_c$ reflex becomes stronger and the intensity ratio increases. Assuming that the area of (112) plus (200) is the same as the area of the (220) in 50:50 mixtures, the cubic content can be calculated by a simple arithmetic operation. The intensity ratios found were 1.823 for ATZ15 and 2.135 for ATZ15P. Thus ATZ15 is entirely tetragonal and ATZ15P contains 7.2 % of cubic in as-sintered state. These results fit well with thermodynamic data. The cubic content of the fractured faces estimated from the intensity ratio of the cubic (111) reflex at 29.55° 2θ and the tetragonal and monoclinic peaks already determined is ~14 area% for ATZ15 and ~21 area% for ATZ15P. Subtracting the initial amount of cubic phase, 14 % of cubic are formed in both cases during phase transformation; this means that the actually transformed fraction of the tetragonal phase is much higher in both cases. A t → m transformation is associated with shear and a higher increase in volume than a t → c transformation with a lower volume increase and

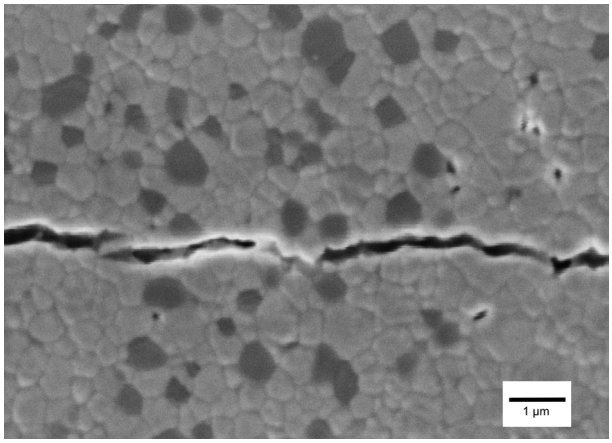

Fig. 7: SEM image of the path of a crack induced by a HV10 indent into polished and thermally etched (1225 °C/1 h air) surface of ATZ15.

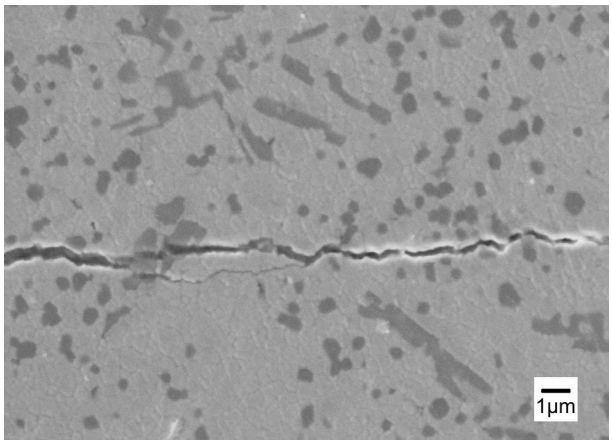

Fig. 8: SEM image of the path of a crack induced by a HV10 indent into polished and thermally etched (1225 °C/1 h air) surface of ATZ15P.

no shear effect. One may conclude that the contribution to toughness of the latter is much smaller and probably negligible. The estimated accuracy of the cubic phase determination is in the range of ± 1.5 % absolute, while the integration error (Table 3) may be neglected.

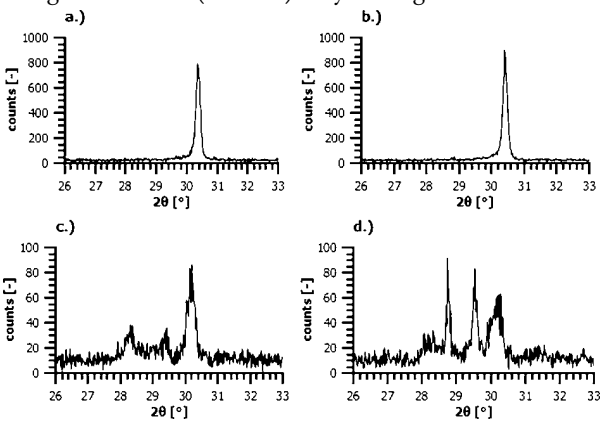

Fig 9: XRD patterns of polished surface and fractured face (2θ = 26-33°):
a.) ATZ15 ground and polished
b.) ATZ15P ground and polished
c.) ATZ15 fracture face
d.) ATZ15P fracture face.

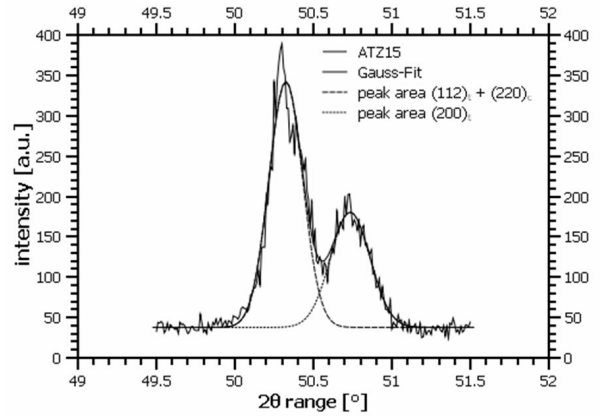

Fig. 10: XRD pattern of polished surface of ATZ15 (2θ = 49.5-51.5°).

Unfortunately after transformation the reflexes in 49.5-51.5° 2θ become very weak and broad so that they cannot be quantitatively interpreted. In both cases the (200) reflex almost completely disappears, which means that the largest fraction of tetragonal is consumed.

In order to obtain a platelet-shape reinforcement, it is important to form the "correct" strontium aluminate phase. Besides the targeted hexaaluminate $SrO \cdot 6\ Al_2O_3$, several other phases such as the dialuminate $SrO \cdot 2\ Al_2O_3$ and monoaluminate $SrO \cdot Al_2O_3$ may be generated during the sintering process. The phase composition in as-fired samples was therefore investigated with XRD. Owing to the high intensity of the zirconia reflexes, a fast scan at 1°/min did not reveal any strontium aluminate phase at all (Fig. 12, overview), even the intensity of a-alumina was very weak compared to the dominant zirconia phase. In order to extract the hexaaluminate signals from the background, the average value of three slow scans at 0.05°/min in the 2θ-range with the strongest strontium aluminate reflex (33.5-34.5°) was determined (Fig. 12, detail). The results of the XRD analysis confirm the formation of the hexaaluminate phase (JCPDS 80-1195), the dialuminate (JCPDS 25-1208) and monoaluminate phase (JCPDS 34-0379) was not detected. This result was expected from the SEM studies showing platelet shape precipitates.

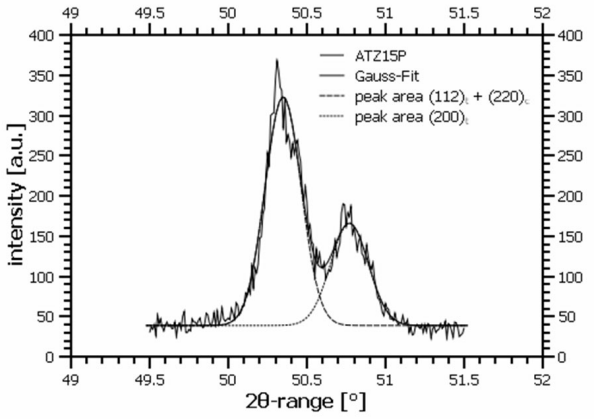

Fig. 11: XRD pattern of polished surface of ATZ15P (2θ = 49.5-51.5°).

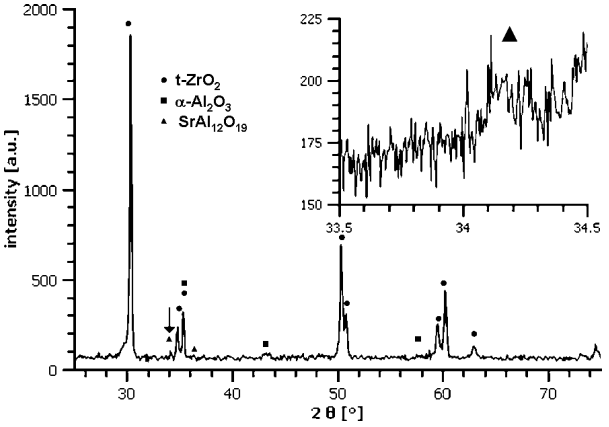

Fig. 12: XRD pattern of sintered ATZ15P.
Overview: (2θ = 25-75°), scan speed 2.5°/min
Detail: (2θ = 33.5-34.5°), scan speed 0.05°/min
Average value of three scans.

IV. Summary and Conclusion

Strontium-hexaaluminate-platelet-reinforced ATZ was manufactured by *in-situ* reacting of strontium zirconate with dispersed alumina. Platelet shape precipitates of 2 – 5 µm in length and 0.5 µm in width are formed. Compared to a standard ATZ of similar recipe, manufactured under the same conditions, the platelet-reinforced material had slightly higher toughness but significantly higher strength and reliability. Weibull-plots of ATZ15 show relatively low reliability in both the as-fired and ground conditions. In ATZ15P Weibull coefficients are considerably higher. Strength of as-fired ATZ15P material is stabilized at a level > 750 MPa.

Tracking of cracks reveals that additional toughness is introduced by crack branching, crack bridging and crack deflection. Besides these expected results, XRD studies show that platelets also increase the transformability of the zirconia by 10 – 15 %. Moreover it was found that during transformation ~ 14 % of cubic phase is formed. ATZ15P initially contains ~7 % of cubic phase while ATZ15 is initially completely tetragonal.

Table 3: Monoclinic contents V_m of polished surfaces and fracture faces transformability and cubic phase content before and after transformation of ATZ15 and ATZ15P.

Material	$V_{m,p}$ polished [%]	$V_{m,f}$ fracture face [%]	Transformability ($V_{m,f}$ - $V_{m,p}$) [%]	$X_{c,f}$ polished [%]	$X_{c,f}$ fracture face [%]
ATZ15	0	22 ± 1	22 ± 1	0	14
ATZ15P	2±1	28 ± 1	26 ± 1.4	7.2 ± 0.1	21

Processing of both materials with injection moulding was possible with identical moulding parameters on a standard injection moulding machine. Defect sizes of the as-fired materials are in the range of 10 µm. The largest flaws are apparently surface defects. After machining, the calculated size of bulk flaws is in the range between 5.8 – 6.8 µm. Platelets help improve the properties of as-fired components. Shifting from a true net-shape forming strategy to a near net-shape strategy with machining of the load-bearing surfaces leads to components with improved mechanical properties and reliability.

Acknowledgements

The authors would like to thank Benjamin Lutz, Andreas Vogel and Willi Schwan for their assistance in injection moulding and sample characterization.

References

1 Chevalier, J., Gremillard, L., Virkar, A.V., Clarke, D.R.: The Tetragonal-Monoclinic Transformation in Zirconia: Lessons Learned and Future Trends, *J. Am. Ceram. Soc.*, **92** [9], 1901-1920, (2009).

2 Hannink, R., Kelly, P., Muddle, B.: Transformation Toughening in Zirconia-Containing Ceramics, *J. Am. Ceram. Soc.*, **83** [3], 461- 87, (2000).

3 Chevalier, J., Cales, B., Drouin, J.M.: Low-Temperature Aging of Y-TZP Ceramics, *J. Am. Ceram. Soc.*, **82** [8] 2150-4, (1999).

4 Chevalier, J., Gremillard, L., Deville, S.: Low-temperature degradation of zirconia and implications for biomedical implants, *Annu. Rev. Mater. Res.* (2007) 37:1-32.

5 Tsubakino, H., Sonoda, K., Nozato, R.: Martensite transformation behaviour during isothermal ageing in partially stabilized zirconia with and without alumina addition, *J. Mater. Sci. Lett.*, **12**, 196-8, 1993.

6 Ross, I.M., Rainforth, W.M., McComb D.W., Scott, A.J., Brydson, R.: The role of trace additions of alumina to yttria-tetragonal zirconia polycrystals (Y-TZP), *Scripta Materialia*, 45 , 6, 653-660, (2001).

7 Tsukuma, K., Ueda, K.: Strength and fracture toughness of isostatically hot-pressed composites of Al_2O_3 and Y_2O_3 partially stabilized ZrO_2, *J. Am. Ceram. Soc.*, **68** [1], C-4-C-5, (1985).

8 Cutler, R.A., Mayhew, R.J., Prettyman, K.M. and Virkar, A.V.: High-Toughness Ce-TZP/AI_2O_3 Ceramics with Improved Hardness and Strength, *J. Am. Ceram. Soc.,* **74** [I] 179-86, (1991).

9 Miura, M., Hongoh, H., Yogo, T., Hirano, S., Fujii, T.: Formation of plate-like lanthanum-β-Aluminate crystal in Ce-TZP matrix, *J. Mat. Sci.* **29**, 262-268, (1994).

10 Burger, W., Richter, H.G.: High strength and toughness alumina matrix composites by transformation toughening and *in situ* platelet reinforcement (ZPTA) – the new generation of bioceramics, *Key Eng. Mat.*, 192-195 , 545-548, (2001).

11 Kern, F., Gadow, R.: Extrusion and Injection Molding of Ceramic Micro- and Nanocomposites, *Int. J. Mat. Forming*, Vol. 2, Suppl. 1, 609-612, (2009).

12 Swain, M.V, Rose, L.R.F.: Strength limitations in zirconia toughened ceramics, *J. Am. Ceram. Soc.*, **69** [7] 511-18, (1986).

13 Casellas, D., Alcala, J., Llanes, L., Anglada, M.: Fracture variability and R-curve behaviour in yttria-stabilized zirconia ceramics, *J. Mat. Sci.*, **36** 3011 – 3025, (2001).

14 Kern, F., El-Ezz, M.A.; Gadow, R.: Thermoplastic Ceramic Injection Molding of Zirconia-Toughened-Alumina Components, in: ICACC34 Daytona Beach, USA, 2010.

15 Opfermann, J., Blumm, J., Emmerich W.-D.: Simulation of the sintering behavior of a ceramic green body using advanced thermokinetic analysis, *Thermochimica Acta*, **318**, 213-220, (1998).

16 Niihara, K.: A fracture mechanics analysis of indentation-induced Palmqvist crack in ceramics, *J. Mat. Sci. Let.*, **2**, 221-223, (1983).

17 Anstis, G.R., Chantikul, P., Lawn, B.R. and Marshall, D.B.A.: A critical evaluation of indentation techniques for measuring fracture toughness. I. Direct crack measurements, *J. Am. Ceram. Soc.*, **64**, 533-538, (1981).

18 Chantikul, P., Anstis, G.R., Lawn, B.R. and Marshall, D.B.A.: A critical evaluation of indentation techniques for measuring fracture toughness. II. Strength method, *J. Am. Ceram. Soc.*, **64**, 539-543, (1981).

19 Toraya, H., Yoshimura, M., Somiya, S.: Calibration Curve for Quantitative Analysis of the Monoclinic-Tetragonal ZrO_2 System by X-Ray Diffraction, *J. Am. Ceram. Soc.*, **67**, 6, C119-121, (1984).

20 Chen, M., Hallstedt, B., Gauckler, L.J.: Thermodynamic modeling of the ZrO_2-$YO_{1.5}$ system, *Solid State Ionics* **170**, 255-274, (2004).